

Coral reef geomorphology of the Spratly Islands: A simple method based on time-series of Landsat-8 multi-band inundation maps



Yanzhu Dong^a, Yongxue Liu^{a,b,c,*}, Chuanmin Hu^d, Bihua Xu^a

^a School of Geography and Ocean Science, Nanjing University, Nanjing, Jiangsu Province 210046, PR China

^b Collaborative Innovation Center of South China Sea Studies, Nanjing University, Nanjing, Jiangsu Province 210046, PR China

^c Jiangsu Center for Collaborative Innovation in Geographical Information Resource Development and Application, Nanjing, Jiangsu Province 210046, PR China

^d College of Marine Science, University of South Florida, St. Petersburg, FL 33701, United States

ARTICLE INFO

Keywords:

Landsat-8 OLI

Coral reef geomorphology

Inundation map

Time series analysis

ABSTRACT

Coral reefs are crucial for the maintenance of the marine ecological environment and for the sustainability of local societies and economies. The use of remote sensing methods with the support of field data has been proposed for mapping coral reef habitats and bathymetry. However, the geomorphology of coral reefs over substantial areas is poorly documented, because of the absence of field data, especially in disputed areas where *in situ* investigation is difficult. In this study, we developed a simple method for mapping the inundation frequency (within the penetration range of optical remote sensing) of coral reefs using time-series Landsat-8 OLI images. The method uses the reef-water reflectance contrast (which varies with bathymetry, bands, and water level) in time-series optical multi-band images in order to derive the inundation frequency and geomorphic zonation of coral reefs. The method was applied to the Spratly Islands—the largest coral reef system in the South China Sea (SCS) using more than 1,100 Landsat-8 OLI images. We established an inventory which comprises 137 reefs/sandbanks/islands, including their spatial extent, inundation frequency, and geomorphic zonation. We also interestingly found that the inundation frequency of reef flats around reclaimed areas has decreased since island construction, which probably reflects the influence of anthropogenic activity on the coral reef ecosystem. Our approach was validated by a study of the Great Barrier Reef in Australia, which demonstrated that the inundation frequency of coral reefs can serve as an indirect representation of their bathymetry.

1. Introduction

Coral reefs are shallow-water calcareous structures accumulated by reef-building corals and the debris of other organisms (Bellwood et al., 2004). Although accounting for less than 1% of the ocean floor, they possess a higher biodiversity than any other marine ecosystem and provide habitats for more than 25% of marine species (Mulhall, 2009). The growth of coral reefs is heavily dependent upon environmental conditions (e.g., temperature, salinity, illumination), and coral bleaching, degradation, and even extinction are usually caused by changes in external environment. In particular, against the background of rapid climate change (including sea surface warming, sea level rise, and ocean acidification) and the intensification of anthropogenic activities (e.g., sewage discharge, over-fishing, diving, and anchoring) (Barkley et al., 2015; De'ath et al., 2012; Hoegh-Guldberg et al., 2007), coral reefs have experienced increasingly severe degradation and decline worldwide since the 1970s (Gardner et al., 2003; Ortiz et al.,

2018). For these reasons, coral reefs are regarded as an important indicator of the health of the marine environment (Butchart et al., 2010; Dodge and Vaišnys, 1975; Shinn, 1966). Increasing awareness has been raised about the preservation and management of coral reef communities (Cinner et al., 2012), because they have a major influence on the maintenance of the global ecological balance (Smith, 1978), as well as on the sustainability of fisheries and tourism (Pauly et al., 2002).

In order to better understand the status of coral reefs and the surrounding marine environment, technologies such as ship-borne echo sounding and Air-borne LIDAR Bathymetry have been developed (Brock et al., 2006; Jung and Vogt, 1992). However, due to limited knowledge of the spatial distribution and underwater topography of coral reefs, it is difficult or dangerous to navigate in the shallow sea areas because of the potential for grounding (Jaap, 2000). Moreover, for islands and reefs located in maritime disputed areas, ships/aircraft are unable to conduct surveys. In these circumstances, therefore, it is unfeasible to carry out detailed, high-frequency field investigations of coral reefs due

* Corresponding author at: Nanjing University, Nanjing, Jiangsu Province 210046, PR China.

E-mail addresses: yongxue@nju.edu.cn (Y. Liu), huc@usf.edu (C. Hu).

to their remote location, complex sea conditions, and the resulting prohibitive expenses, leading to a deficiency or even absence of field data in the spatio-temporal domain.

Satellite remote sensing (RS) technology enables the remote and recurring global-scale observation of large areas (Stone, 2010; Wulder et al., 2012). Previous studies have shown the capability of optical RS methods for mapping coral reef geomorphology/benthic-habitat by processing one or multiple images (Ahmad and Neil, 1994; Leon and Woodroffe, 2011; Phinn et al., 2012; Roelfsema et al., 2018; Zhang, 2015). The coral reef geomorphic zonation in remote and disputed seas (where field data is usually absent or publicly unavailable) is yet to be a challenging topic (Chen et al., 2019). Time-series optical multi-band images (e.g., the Landsat-8 Operational Land Imager (OLI)) with the improving geolocation accuracy provide detailed information over time (Wang et al., 2019), and thus, may offer an opportunity to map coral reef geomorphology in such areas.

Inundation mapping for terrestrial ecosystems generally means the delineation of a flooded area. In this study, we use the term “inundation” as a proxy for demonstrating the coral reef geomorphology: it can be easily discerned that whether coral reefs are physically flooded or exposed from SWIR bands; and from the blue and green bands, more parts of coral reefs underwater can be “seen” due to their greater penetration ability. In other words, taking the penetration depth of different bands as base surfaces, coral reef can generally be divided into “inundated (unseen)” or “exposed (seen)”. And the “inundation frequency” derived from time-series multi-band images can represent which part of coral reef is more often “seen” or “unseen” in different bands over time.

The objectives of this study are two-fold: (i) To develop a method of mapping the inundation frequency of coral reefs from time-series Landsat-8 OLI images; and (ii) To generate an inventory (including number, distribution, inundation frequency, and geomorphic zones) of coral reefs in the Spratly Islands—the largest coral reef system in the South China Sea (SCS). The article is organized as follows: Section 2 briefly describes the Spratly Islands and the datasets used; Section 3 introduces the methods for mapping coral reef inundation; Section 4 presents the results of the monitoring of inundation frequency of the coral reefs in the Spratly Islands; and Section 5 discusses the implications, transferability, and reliability of the derived inundation maps.

2. Study area and datasets

2.1. The Spratly Islands

The SCS is a marginal sea in the western Pacific Ocean, occupying an area of $\sim 3.5 \times 10^6 \text{ km}^2$, and extending from 3°S to 23°N (Su, 2004). The area of coral reefs in the SCS is $\sim 3.8 \times 10^4 \text{ km}^2$, constituting around 5% of the world's coral reefs (Wang et al., 2014). Coral reefs in the SCS are mainly distributed in the Spratly Islands, Scarborough Shoal, Macclesfield Bank, the Paracel Islands, and the Pratas Islands, from south to north (Fig. 1a). Within the SCS, the Spratly Islands are the southern-most archipelago with the largest number and widest distribution of coral reefs. According to incomplete statistics, there are more than 100 islands, atolls, sandbanks, shoals and reefs in the Spratly Islands (Zhong, 1996), most of which are submerged at high water, and some are submerged even during the lowest tides. Notably, the Spratly Islands have not been systematically investigated so far due to the maritime disputes over the area, and the exact number of coral reefs remains unclear (relevant studies are summarized in Table S1 of the Supplementary Material). Therefore, increasing our knowledge of the extent, distribution, and inundation of coral reefs in the region is important for navigation safety assurance and marine environmental protection.

2.2. Satellite datasets

The Operational Land Imager (OLI) onboard the Landsat-8 satellite collects images with a 16-day revisit cycle and a 30-m resolution for the visible and infrared bands (Bands 1–7). Landsat-8 OLI data are quantized to 12 bits and provide a higher Signal to Noise Ratio (SNR) than data acquired by its predecessors (USGS, 2018), which enables better discrimination between coral reefs and water. The geometric performance of Landsat-8 OLI images over oceans is also satisfactory (the geometric accuracy of OLI images can be 18 m, with a circular error of 90%) (Liu et al., 2019).

The Spratly Islands are covered by a total of 16 tiles from world reference system 2 (WRS-2) of Landsat-8 OLI images (path: 118–122, row: 52–56, Fig. 2a). In order to acquire the inundation frequency of each coral reef from a relatively long and continuous time series, a total of 1,138 scenes of OLI Level-1 images were downloaded from Earth Explorer of the United States Geological Survey (USGS) (<https://earthexplorer.usgs.gov/>). The time span of acquired Landsat-8 OLI images is from 23 April 2013 to 31 December 2017. Considering that the Spratly Islands area is frequently affected by clouds, pixels covered by cloud were excluded and the data usability frequency (i.e., frequency of cloud-free data) over the area was calculated (Fig. 2a). Over 92% of the study area was covered by > 40 cloud-free observations (Fig. S1 of the Supplementary Material).

2.3. Global dataset of coral reefs

Moderate spatial resolution satellite data have been used to map the geomorphology of coral reefs worldwide, such as the Millennium Coral Reef Mapping Project (Andréfouët et al., 2006) and the UNEP-WCMC (United Nations Environment World Conservation Monitoring Centre) coral reef inventory (UNEP-WCMC et al., 2018). In this study, we used the UNEP-WCMC inventory (Version 4.0, by 2018) as a reference source, which provides the most comprehensive global distribution of coral reefs in tropical and subtropical areas and the data sources include the Millennium Coral Reef Mapping Project. Note that (i) In case of the Spratly Islands, the area of coral reefs in the inventory is $\sim 13.5 \text{ km}^2$, which is much smaller than is known; (ii) The spatial resolution of the raster inventory is relatively coarse ($\sim 500 \text{ m}$), and consequently the outlines of the coral reefs are usually jagged; (iii) The locations of coral reefs in the inventory are usually offset from their actual locations (e.g., for Xiyue Island the deviation can be up to $\sim 500 \text{ m}$, as can be seen in Fig. S2d of the Supplementary Material); and (iv) Several tens of coral reefs are omitted from the inventory of the Spratly Islands (see Table S2 of the Supplementary Material), which may be attributed to the process of cartographic generalization.

2.4. High resolution images and historical data

The shape and geomorphic characteristics of coral reefs in clear seawater can be readily identified in high resolution (HR) images (Fig. 4a1–c1). Historical HR images during 2013–2017 on Google Earth (GE) were used to complement the aforementioned global coral reefs inventory. Careful visual inspection of the available images was used to examine the location and existence of coral reefs in the Spratly Islands. The geographical names of the Spratly Islands recorded in historical data (Geographical Names Committee of Guangdong Province, 1987), in both Chinese and English, were collected as evidence. Notably, the existence of recorded coral reefs needs to be confirmed further given that some of them are located in deep water ($> 30\text{-m}$ depth) which is beyond the penetration of optical remote sensing. A unique identifier was assigned to each coral reef in sequence for convenience in data processing.

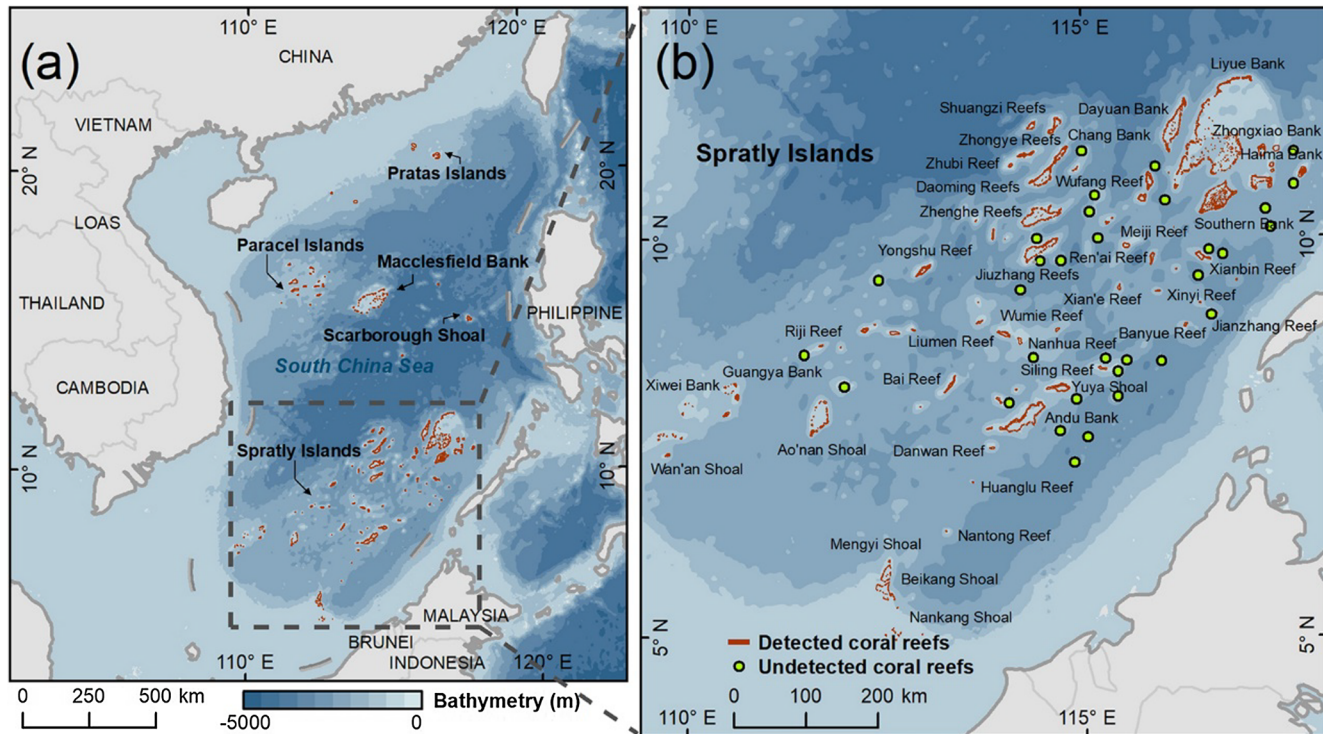


Fig. 1. (a) The South China Sea, showing the location of the Spratly Islands in the southern SCS. (b) Enlarged view of the Spratly Islands, showing the spatial distribution of detected and undetected coral reefs based on the inventory built in this study.

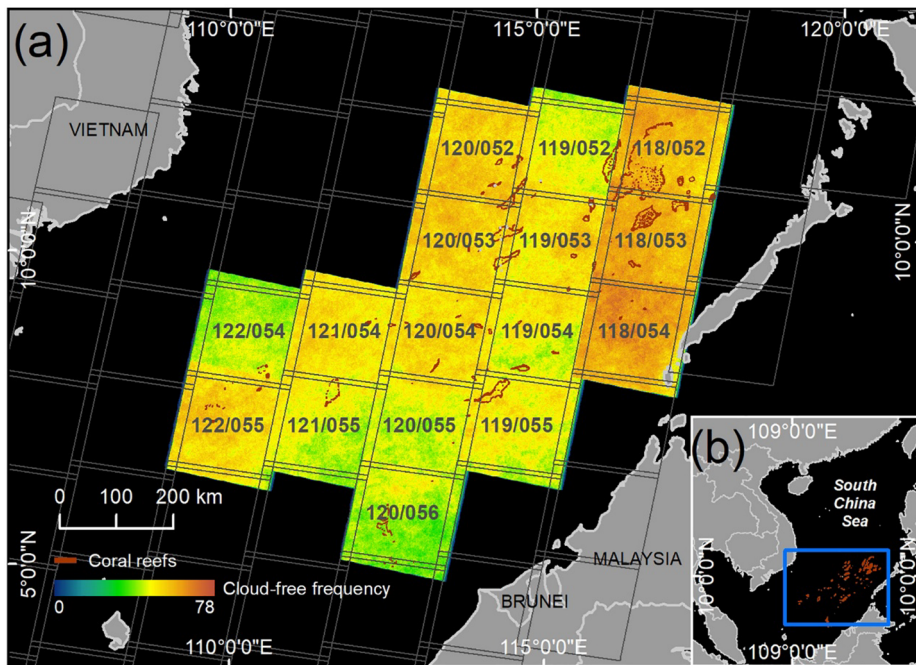


Fig. 2. (a) Landsat data tiles and data usability (i.e., cloud-free frequency) of Landsat-8 OLI images from 23 April 2013 to 31 December 2017 for the Spratly Islands. (b) Location of the Spratly Islands.

3. Methodology

3.1. Strategy for detecting coral reef inundation frequency from time-series OLI images

The contrast in reflectance between coral reefs and the surrounding water was used to map the inundation of coral reefs from time-series satellite images. Assuming that the coral reef geomorphology usually

changes slightly within a relatively short period, the reflectance of coral reefs and the surrounding background (i.e., seawater) exhibits varying degrees of contrast which depend mainly on bathymetry, bands, and water level.

- (1) *Variation of contrast with bathymetry.* For a given optical band, the reflectance observed above the water surface varies spatially as a result of bathymetric modulation, and the spectral ability to

distinguish inundated coral reefs from the surrounding water decreases gradually with increasing water depth. Here, the inundated parts of coral reefs refers to the parts above the maximum penetration depth of the optical band. Given that both the optical properties of open ocean waters (e.g., the Spratly Islands, hundreds of kilometers from the mainland) and the performance of the sensor remain stable, areas of inundation exhibited within a given band will be mainly influenced by water depth. Admittedly, the island reclamation activities such as dredging and filling may permanently alter the bathymetry of local coral reefs and surrounding areas (Barnes and Hu, 2016), but the bathymetry can be assumed to be stable before and after construction, and the implication of which is further discussed in Section 5.4.

- (2) *Variation of contrast between bands.* For a given OLI image, there is a spectral difference of penetration ability among different wavelengths. The longer the wavelength, the weaker the capability of penetrating water due to the attenuation of radiation. Specifically, the blue band (Band 2, 450–515 nm) penetrates the farthest and can reach depths of up to 20–30 m depending on water clarity. The green band (Band 3, 525–600 nm) can penetrate to a maximum depth of ~15 m, the red band (Band 4, 630–680 nm) to ~5 m, the near-infrared band to ~0.5 m (Band 5, 845–885 nm), and the shortwave-infrared (SWIR) band (Band 6, 1,560–1,660 nm) is unable to penetrate the water surface due to the strong absorption effect (Jupp, 1988). Therefore, the area of inundation for a given reef decreases with increasing wavelength (Fig. 3a1–a4). Notably, (i) Although OLI possesses another blue band (Band 1, 433–453 nm), measurements in coral reef waters indicate that Band 2 penetrates deeper than Band 1 (Zhao et al., 2013); (ii) Band 5 was not used because white caps generated by breaking waves against the shallow reef flats would be misidentified as exposed coral reefs from this band, while Band 6 is less uninfluenced by white caps (Fig. S3 of the Supplementary Material); and (iii) The penetration depths for different bands may be specific to different coral reef

areas due to the variation of the inherent optical properties. As for the Spratly Islands—which are located in open ocean hundreds of kilometers from the mainland, MODIS K_d (490) during 2013–2017 from four separated sites of the study area remains very low and relatively stable ($0.04 \pm 0.02 \text{ m}^{-1}$) (Fig. S4 of the Supplementary Material), very close to the clearest Caribbean coral reef waters ($\sim 0.03 \text{ m}^{-1}$).

- (3) *Variation of contrast with water level.* The periodic rise and fall of sea level caused by tidal action changes the spatial extent of the inundated coral reefs, which moves back and forth accordingly (Liu et al., 2013). The varying areas of inundation that appear in the time-series images can be seen as different contour planes of the coral reef topography (Fig. 3a–c). Admittedly, the water depth of intertidal reef may also influenced by some other natural factors (e.g., storms, gyres, and El Nino events) that happen occasionally and ephemerally. Note that from the perspective of dozens of satellite observations, the occasional constitutes (these disturbances usually appear randomly) can be mitigated, and the periodic constitutes (they usually present position-invariant characteristic) will be enhanced by the following time-series operation.

According to the position-invariant characteristic of coral reefs and the adequate geometric accuracy of OLI images (~18 m), it is possible to accumulate time-series results of inundation and false positives (e.g., clouds) in each image can also be excluded effectively. The bathymetry of coral reefs can be better depicted by accumulating inundation results from Bands 2–4 and Band 6, in order to make full use of the contrast provided by different spectral bands (Fig. 3d). The maximum inundation extent of coral reefs can also be obtained from the inundation time-series. The higher inundation frequency of pixels implies that they are more often “inundated” (detected by optical RS more times in all bands), and thus they should be located at a shallow water depth. By contrast, pixels with lower inundation frequency are assumed to be deeper.

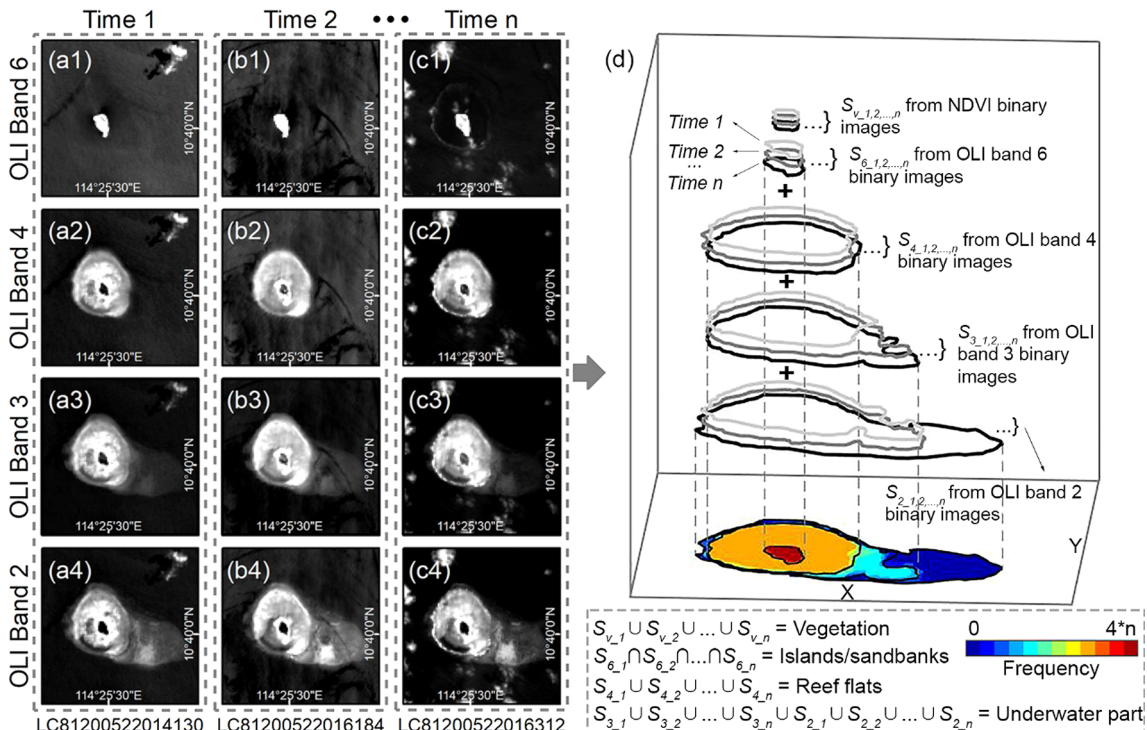


Fig. 3. (a–c) Comparison of inundation in Landsat-8 OLI bands 2–4 and band 6 on three different dates. (d) Diagram showing the accumulation of inundation using different bands. The maximum frequency is 12 for this example of three different scenes. The formulas in the dashed box describe the principles used to determine different geomorphic zones of coral reefs. $S_{v,1,2,\dots,n}$ are the areas of vegetation from NDVI binary images of Time 1,2,...,n; and $S_{2,1,2,\dots,n}$, $S_{3,1,2,\dots,n}$, $S_{4,1,2,\dots,n}$ and $S_{6,1,2,\dots,n}$ are the areas of inundation from OLI Bands 2, 3, 4, and 6 binary images of Time 1,2,...,n, respectively.

We categorized the coral reefs of the Spratly Islands into four geomorphic zones based on different bands and their combinations: (i) *Underwater parts*. The blue band (Band 2) and green band (Band 3) provide the most comprehensive underwater information and the part always below the water surface, including hidden reefs, shoals, banks and lagoons, can be derived by the union of all time-series of binary images from Band 2 and Band 3; (ii) *Reef flats*. Lying in the inter-tidal zones, reef flats may be exposed to air during low tide and can be distinguished from the union of the red band (Band 4, with a penetration depth of ~5 m for clear water) inundation time-series, because these areas exhibit much higher frequency than the surrounding water; (iii) *Exposed part of coral reefs*. These are above the sea surface even during high tides and can be extracted from the SWIR band (Band 6, no penetration), including exposed rocks, sandbanks, and natural and artificial islands (Here, the artificial islands are defined as portions converted from submerged coral reefs by anthropogenic activities (Barnes and Hu, 2016)). The exposed areas, which vary with the water level, can be derived from the intersection of all time-series of binary images from Band 6; and (iv) *Vegetated area*. As can be seen in Fig. 3a2–a4, the reflectance of vegetation on the islands is lower than that of submerged coral reefs in Bands 2–4, and the area of exposed vegetation can be extracted from the union of all time-series of Normalized Difference Vegetation Index (NDVI) results which utilize the ratio of Band 4 and 5 (Townshend and Justice, 1986). A comparison of HR images and OLI bands that demonstrate the characteristics of different geomorphic units is shown in Fig. 4. Section 3.2 provides a detailed description on the process of determining each geomorphic part of coral reefs. Notably, the feasibility and compatibility of the proposed classification

scheme in some geomorphologically complex coral reef areas need to be further investigated.

3.2. Procedure for mapping coral reef inundation frequency in the Spratly Islands

Based on the aforementioned spectral characteristics and the accumulation strategy for acquiring inundation frequency from time-series OLI images, a method was developed to map the inundation frequency of coral reefs in the Spratly Islands. The steps are described as follows:

- (1) *Step 1: Data pre-processing* (Fig. 5a). Pre-processing procedures of Landsat 8 OLI images were automatically implemented in two sub-steps: (i) The relative digital number (DN) in the original images was first converted to the absolute top-of-the-atmosphere (TOA) radiance. TOA radiance was then converted to above-water reflectance in order to minimize the influence of the atmosphere and aerosols using the atmospheric correction model FLAASH embedded within the ENVI software. (ii) Cloud masks were generated based on the Quality Assessment (QA) bands of OLI images in order to eliminate the influence of cloud. To avoid possible omission and false detection in the QA bands, the areas of “cloudy” pixels were dilated with a radius of five pixels.
- (2) *Step 2: Traversal and sub-setting* (Fig. 5b). Considering the large amount of data covering the Spratly islands, it was necessary to subset small image chips of interest from the entire dataset in order to reduce the computing time required for classification. In order to determine all potential coral reef areas, the mean filtering results of

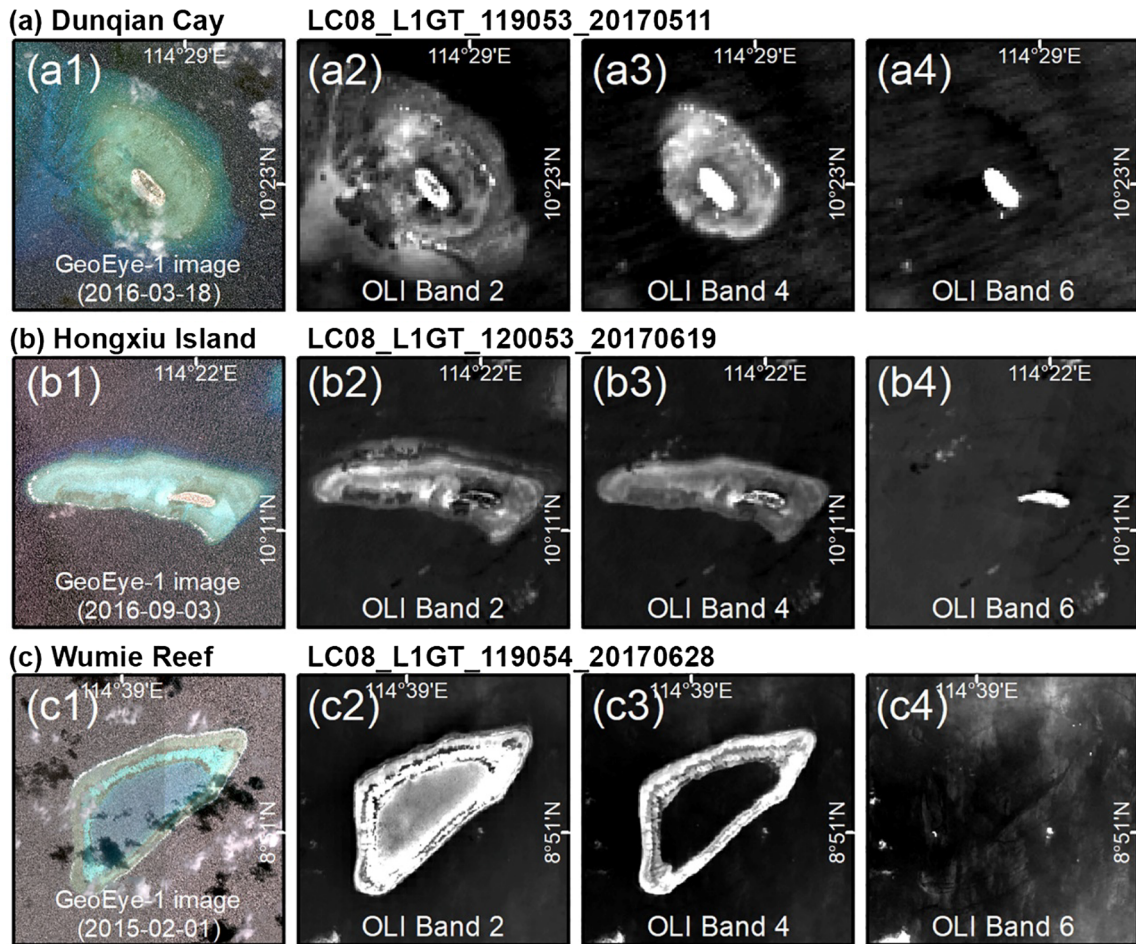


Fig. 4. Comparison of GeoEye-1 satellite images and Landsat-8 OLI Bands 2, 4, and 6 (Band 3 is not shown here because of the similar inundation as Band 2; however, Band 3 was used to map the inundation of coral reefs). HR images acquired in the same year were used due to the availability of HR images.

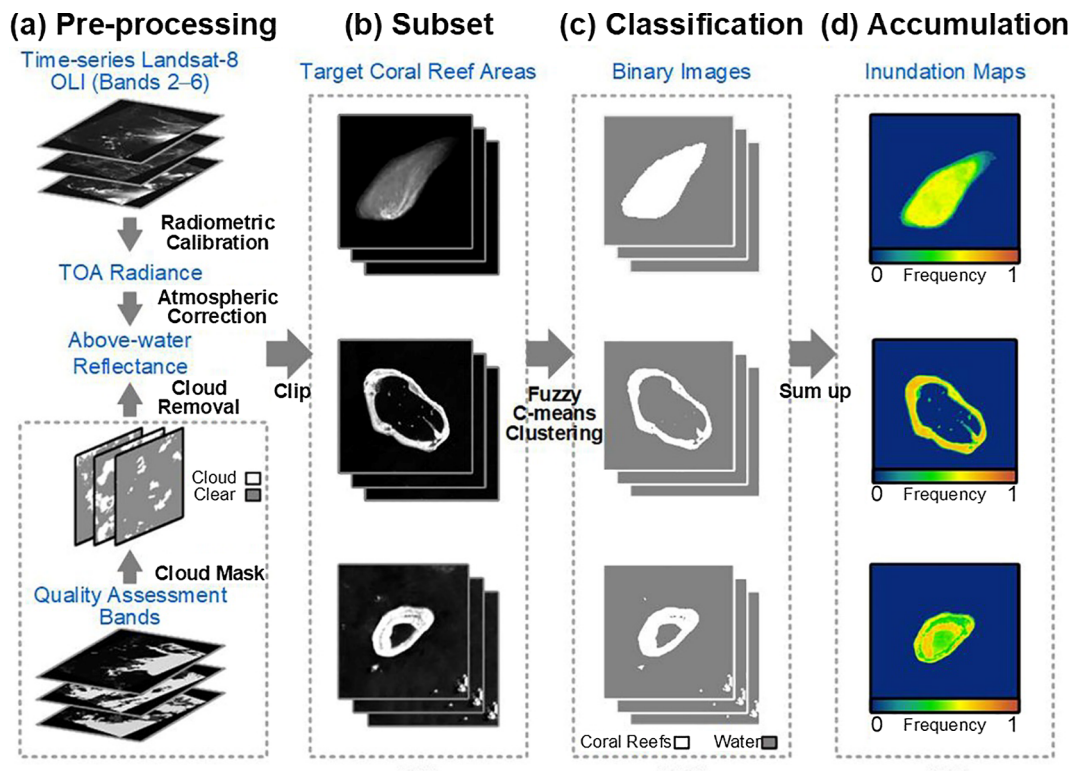


Fig. 5. Flowchart showing the process of mapping the inundation frequency of coral reefs from time-series Landsat-8 OLI images. In this example, three targets are selected to show the accumulated inundation frequency after normalization to the number of cloud-free observations.

OLI Band 2 (blue band) were first calculated within a specified circular neighborhood (the radius of the neighborhood was set empirically to 40 pixels), and then subtracted from the original DN values of Landsat-8 OLI scenes in order to intensify the difference between coral reefs and seawater. Binary images of coral reefs from time series were segmented from the subtraction results, and were then accumulated. By accumulating the subtraction results from the time series, coral reefs with brighter values can be clearly discriminated from the dark seawater background. Careful visual examination of the accumulation results tile by tile was conducted in order to determine all of the target areas of coral reefs.

(3) *Step 3: Classification* (Fig. 5c). In the blue and green bands, the contrast between the underwater parts of coral reefs and the surrounding water becomes subtler with increasing water depth. This phenomenon makes it difficult to delineate the boundaries between underwater reefs and water. Conventional hard clustering methods divide pixels into distinct classes, in which each pixel can only be assigned to one class. By contrast, fuzzy c-means (FCM) clustering is capable of calculating the proximity of a pixel to each class and to assign the pixel to the class with the highest degree of probability (Ghosh et al., 2011; Yang et al., 2015). We adopted the FCM clustering method to segment the underwater parts of coral reefs from the OLI images and generate binary images of extracted coral reefs. Further details about the automated method for water segmentation are given in Yang et al. (2015). Admittedly, this technique is still insensitive to false signals (e.g., clouds, waves, and sun glint) in OLI images. All of the binary image chips were visually inspected and only those that had been correctly classified were retained for accumulation.

(4) *Step 4: Time-series accumulation* (Fig. 5d). The time-series of binary images of inundation from each band were first accumulated for each coral reef respectively, and then the results from OLI Bands 2–4 and Band 6 were accumulated together. False positives such as clouds with relatively low frequency were eliminated by manual

inspection. In order to make the results between different coral reefs more comparable, the inundation frequency was converted to the probability of inundation with a range from 0 to 1 by dividing the number of cloud-free observations at each pixel. A specific example of the time-series accumulation process is shown in Fig. S5 of the *Supplementary Material*. The geomorphic zones of coral reefs were also acquired by taking the union or intersection of time-series binary images of each band, or the combination of bands, according to the principles described in Section 3.1, and then the areas of each geomorphic zone were calculated. Examples of the zoning process under different conditions are shown in Fig. S6 of the *Supplementary Material*.

4. Results

4.1. Inventory of coral reefs in the Spratly Islands

An inventory was established to quantify the abundance and distribution of coral reefs in the Spratly Islands. According to the detection results from time-series Landat-8 OLI images acquired between 2013 and 2017 (a total of 1,138 scenes), coral reefs in the Spratly Islands cover an area of almost $2.5 \times 10^3 \text{ km}^2$ (the areas within the detection range of optical RS). The distribution of coral reefs in the Spratly Islands is concentrated in the northeast and is relatively scattered in the southwest, extending from Nankang Shoal ($\sim 5^\circ\text{N}$) in the south to Liyue Bank ($\sim 11^\circ\text{N}$) in the north, and from Wan'an Bank ($\sim 109^\circ\text{E}$) in the west to Haima Bank ($\sim 117^\circ\text{E}$) in the east (Fig. 1b). The enumeration principle for the coral reefs conforms to the historical nomenclature system in the Spratly Islands, which considers a variety of factors, including the degree of exposure, geomorphological structure, and the spatial correlation of coral reefs. Based on the aforementioned principles, a total of 137 reefs, islands, sandbanks, shoals, and banks were detected from the time-series OLI images of the Spratly Islands. The complete list of detected coral reefs and a table listing their Chinese and English names

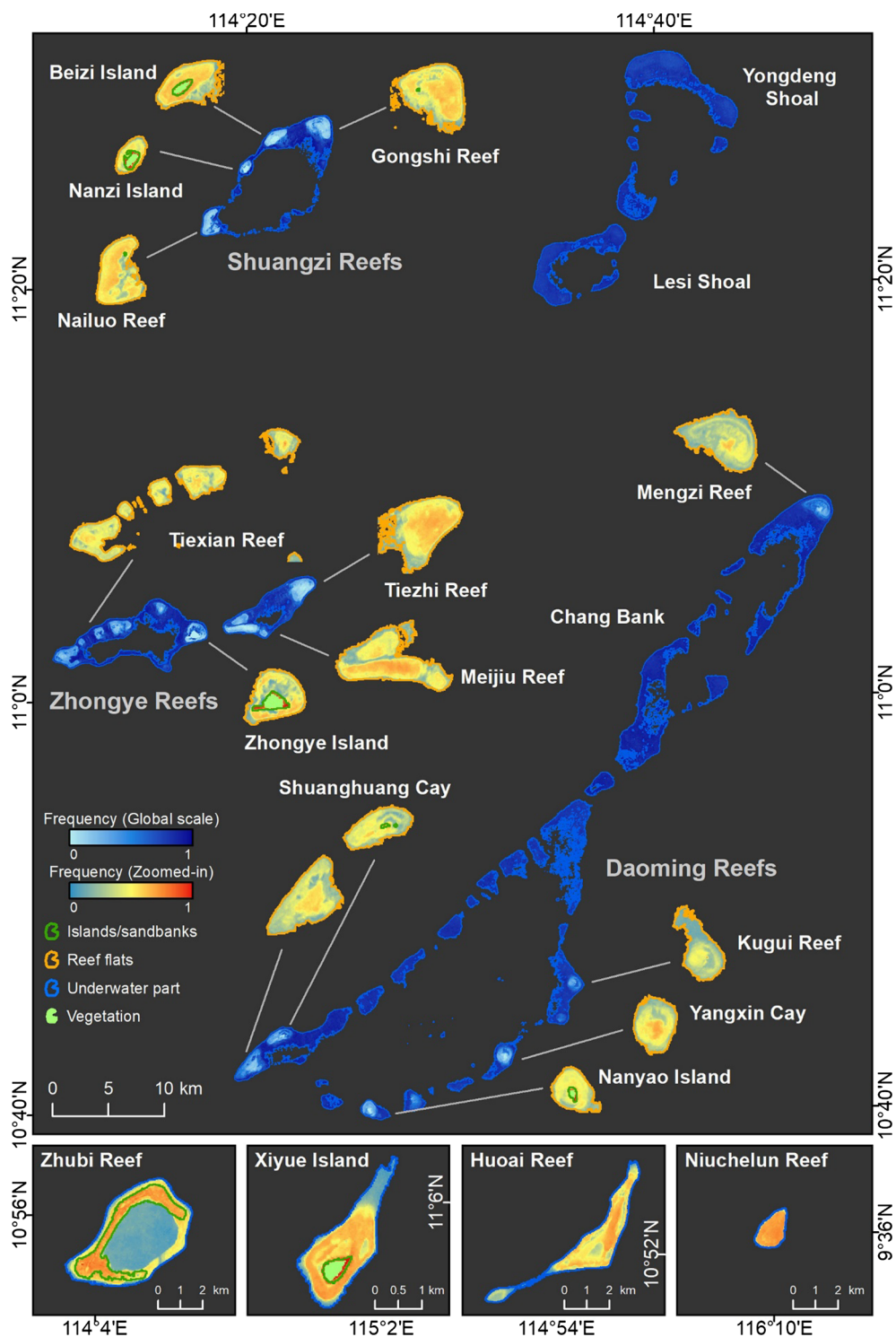


Fig. 6. Inundation map including Shuangzi Reefs, Zhongye Reefs, Daoming Reefs and other isolated coral reefs in the northern part of the Spratly Islands.

are given in Table S3 of the [Supplementary Material](#). For convenience, all of the coral reefs are henceforth described using their Chinese names.

Since it was not feasible to conduct an *in situ* validation of each coral reef in the proposed inventory, other datasets were used as a reference to compare with the results of the time-series accumulation approach. The geographical locations of coral reefs extracted from OLI images accord well with their actual locations in historical HR images available on GE (from 2013 to 2017). It was found that four reefs/banks were detected but are not recorded in the historical data. One is part of the

Daoming Reefs, between Nanyao Island and Yangxin Cay in Fig. 6; another is part of the Jiuzhang Reefs, between Zhangxi Reef and Biansheng Reef in Fig. 7; and the other two are located to the southeast of Zhongxiao Bank and northwest of Haima Bank in Fig. 8, which were previously ignored because of their relatively low inundation frequency. In addition, a total of 32 reefs/shoals (1 from the UNEP-WCMC dataset, 19 from an historical atlas ([Geographical Names Committee of Guangdong Province, 1987](#)), and 12 from both) were recorded in the UNEP-WCMC dataset or historical data, but were undetected from the time-series OLI images (Fig. 1b); they may have been submerged at a

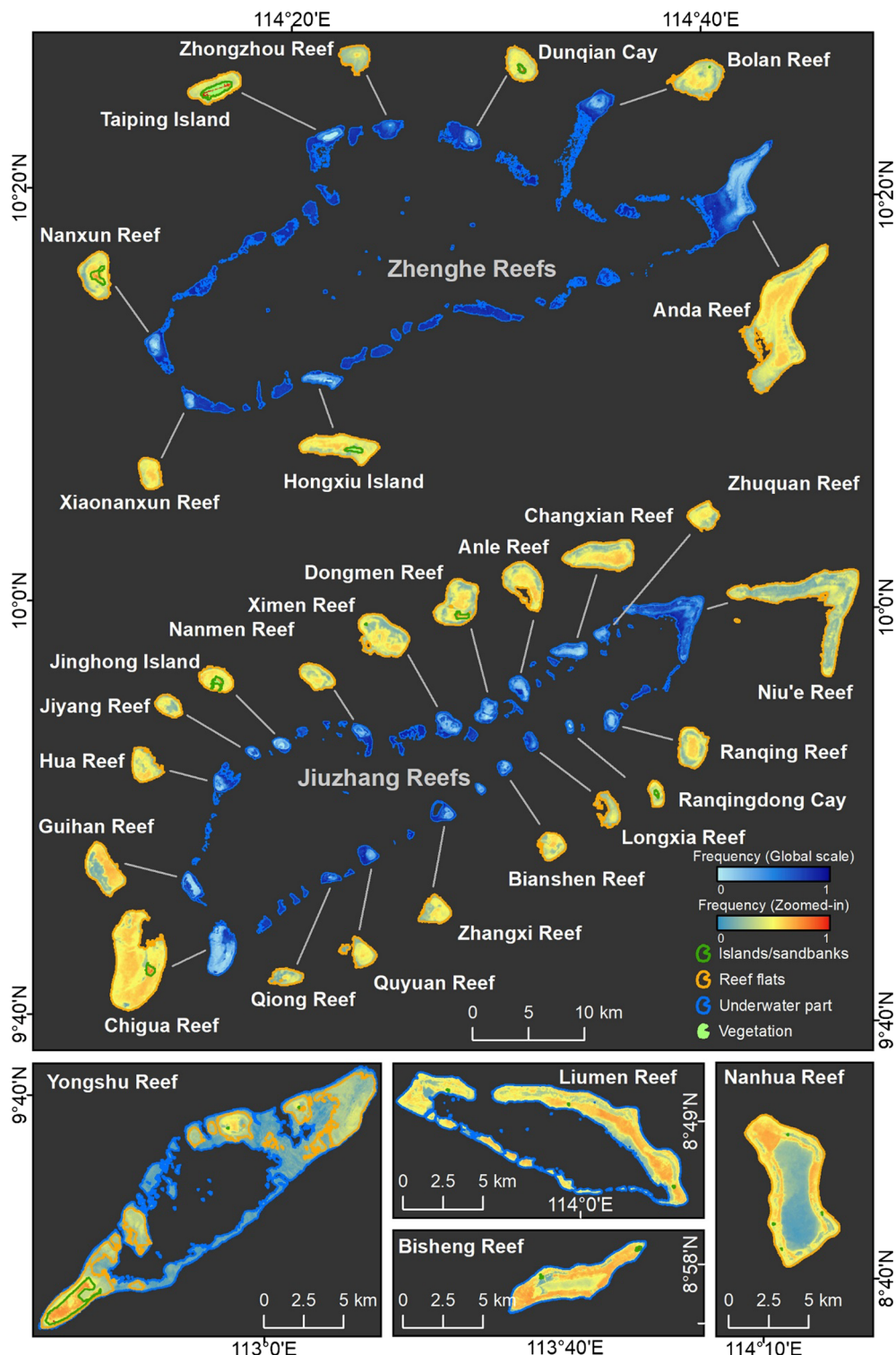


Fig. 7. Inundation map including Zhenghe Reefs, Jiuzhang Reefs and other isolated coral reefs in the Spratly Islands.

depth exceeding the detection range of optical RS. The existence of the undetected coral reefs was further determined by visually inspecting all of the available Landsat-5 Thematic Mapper (TM) images (from 1 January 1984 to 1 January 1999, 1,778 scenes) and Landsat-7 Enhanced Thematic Mapper plus (ETM+) images (from 1 January 1999 to 23 April 2013, 745 scenes). The geometric accuracy of satellite images acquired by early launched satellites may not be sufficiently accurate (Liu et al., 2019), and therefore we conducted a visual inspection using a 10-km radius around the undetected coral reefs. As a result, none of

the 32 coral reefs were discovered in all TM/ETM+ images available; i.e., only 137 coral reefs could be detected from the perspective of optical remote sensing (Figs. S7-10 of the Supplementary material).

4.2. Maps of inundation frequency

An “inundated” status means that part of the coral reefs is within the penetration range of visible light, which can be discriminated based on the reflectance contrast between submerged coral reefs and the

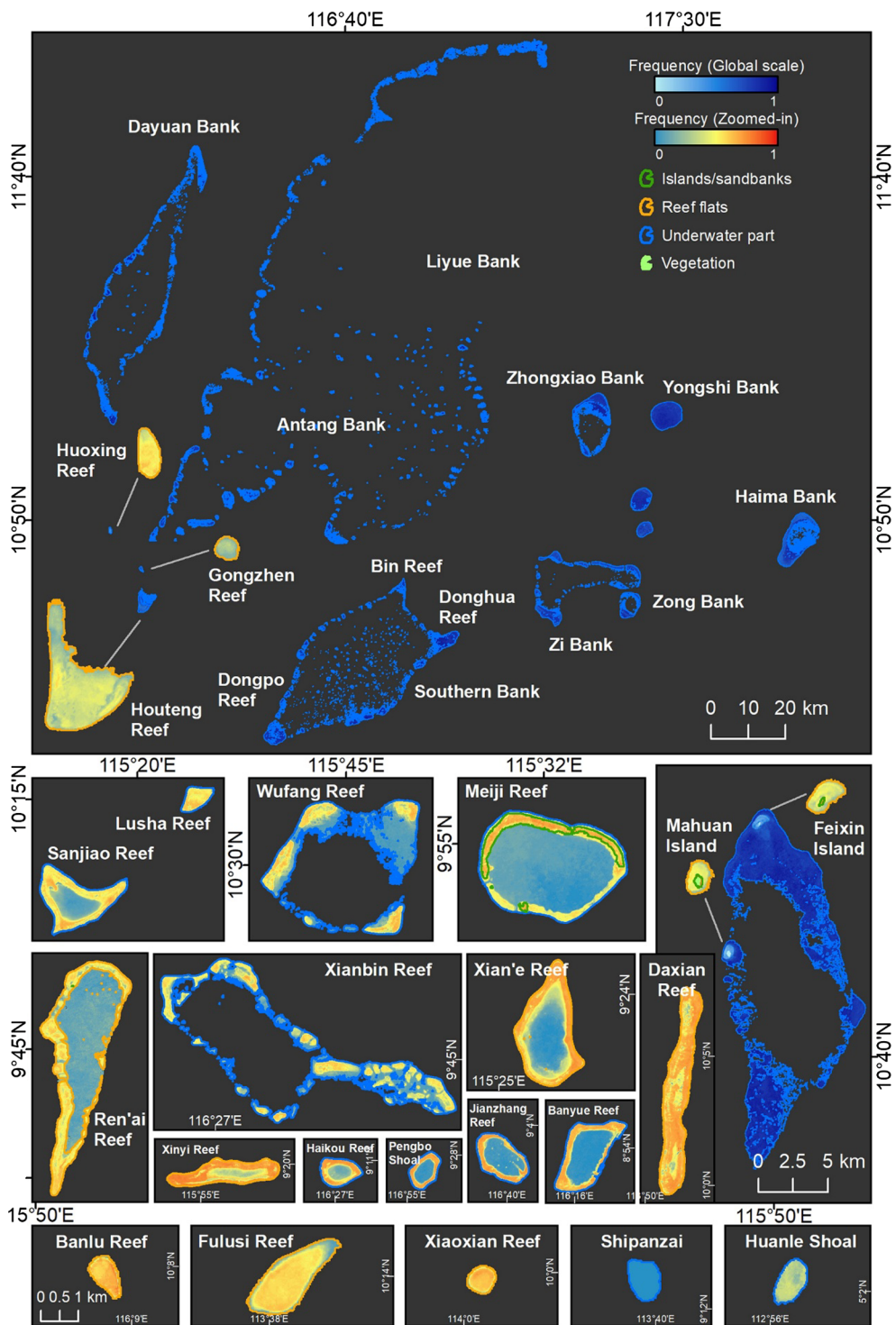


Fig. 8. Inundation map including coral reefs in the northeastern part of the Spratly Islands and other isolated coral reefs.

surrounding water in OLI images. Binary images of the inundated part (i.e., submerged coral reefs) and non-inundated part (i.e., water) were generated using the FCM method. The areas of inundation for each coral reef varied between images acquired on different dates and different bands. By accumulating binary images of inundation from time-series OLI Bands 2–4 and Band 6 images, the inundation frequency of the coral reefs was determined, which depicted variations in inundation in both the temporal and spatial domains. A data normalization procedure was applied to the entire area by dividing the inundation frequency by the data usability frequency for each pixel.

Final inundation frequency maps of coral reefs in the Spratly Islands are shown in Figs. 6–9. As can be seen, on a global scale, the frequency of coral reefs from high to low values is displayed as a color gradient (from light-blue to dark-blue) in order to depict the actual variation of the bathymetry. The dark blue boundaries surrounding the coral reefs represent the extent of maximum inundation (i.e., the union of time-series of inundation areas from OLI Bands 2–4 and 6). The zoomed-in parts in the inundation maps correspond to reef flats that may be exposed to the air at low tide. The frequency of reef flat areas is shown using a different type of color scheme (from cold-blue to warm-red) and

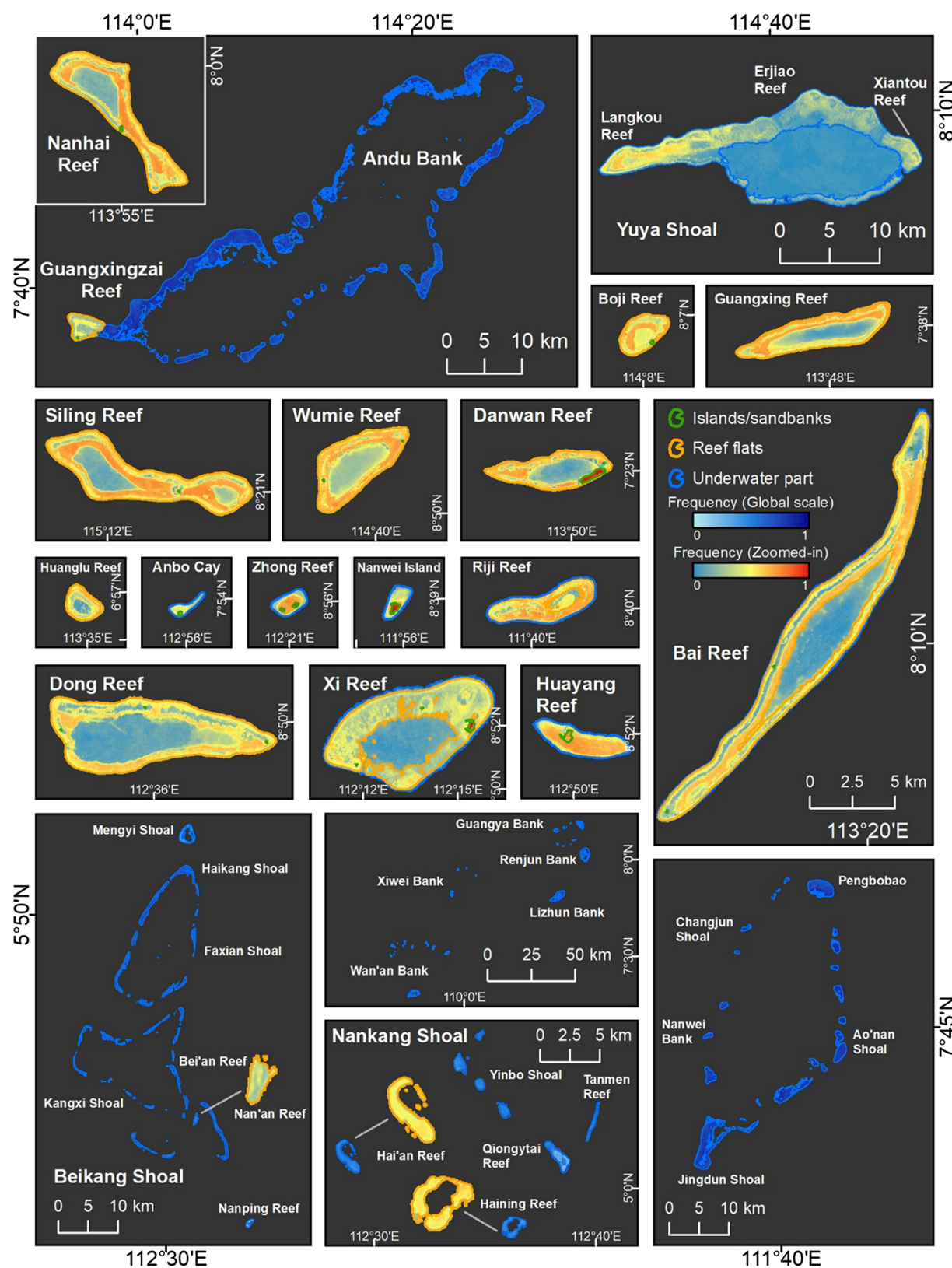


Fig. 9. Inundation map including Beikang Shoal, Nankang Shoal, and other reefs/shoals/banks in the southwestern part of the Spratly Islands.

their boundaries are delineated in orange. Permanently exposed areas (the intersection of time-series of inundation areas from OLI Bands 2–4 and 6), such as islands/sandbanks exhibit the highest frequency in the inundation maps, and their boundaries are shown in dark green. The

inundation frequency of coral reefs decreases gradually from the highest topographic point to the surroundings, and they vary spatially in a similar pattern to the underwater topography. Vegetated areas are shown in light green.

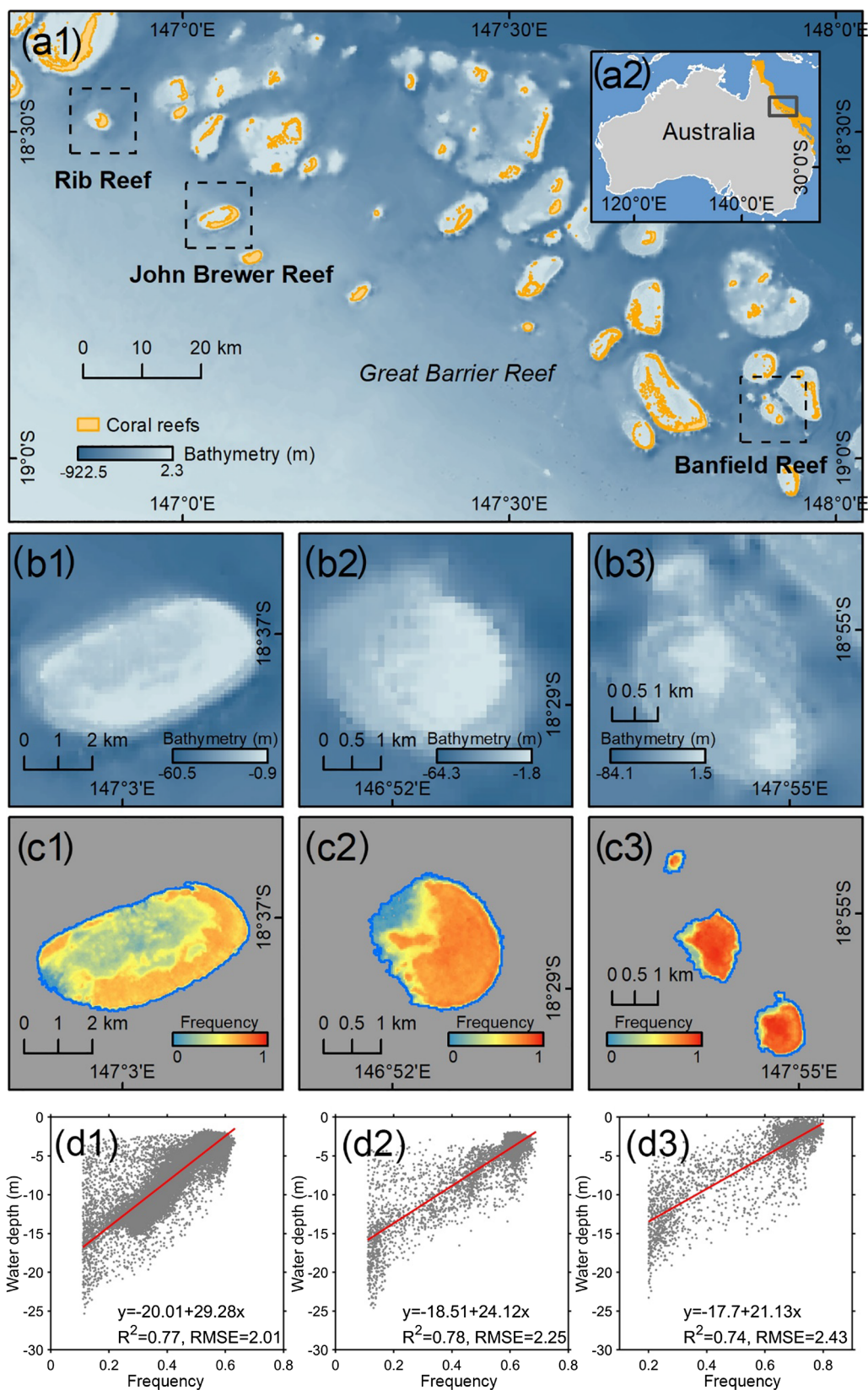


Fig. 10. (a1) Location of selected test sites in the GBR. (b1–b3) Bathymetric data for the three test sites. (c1–c3) Inundation frequency at the three test sites. (d1–d3) Scatterplots and fitted regression lines for the relationship between frequency and water depth at the three test sites.

Table 1
Area statistics of coral reef geomorphic zones in the Spratly Islands.

Name	S_i (km^2)	S_v (km^2)	S_f (km^2)	S_u (km^2)	Name	S_i (km^2)	S_v (km^2)	S_f (km^2)	S_u (km^2)	Name	S_i (km^2)	S_v (km^2)	S_f (km^2)	S_u (km^2)
Xiaoxian Reef	0.00	0.00	0.43	0.00	Jianzhang Reef	0.00	0.00	4.52	4.62	Xi Reef	0.23	0.00	25.62	16.24
Banlu Reef	0.00	0.00	0.61	0.00	Riji Reef	0.01	0.00	7.43	2.55	Zhongye Reefs**	0.47	0.28	20.76	24.81
Huanle Shoal	0.00	0.00	0.73	0.00	Dawan Reef	0.45	0.00	5.93	4.68	Meiji Reef	5.94	0.00	7.78	33.67
Shipanzai	0.00	0.00	0.76	0.00	Sanjiao Reef	0.00	0.00	8.17	3.85	Yongshi Bank	0.00	0.00	0.00	48.92
Nanping Reef	0.00	0.00	0.96	0.00	Zong Bank	0.00	0.00	12.83	0.00	Renal Reef	0.01	0.00	18.35	32.45
Anbo Cay	0.04	0.00	0.57	0.43	Guangxing Reef	0.00	0.00	8.51	5.37	Antang Bank	0.00	0.00	0.00	52.31
Huoxing Reef	0.00	0.00	1.12	0.00	Bisheng Reef	0.09	0.00	10.46	3.38	Zi Bank	0.00	0.00	0.00	53.52
Haining Reef	0.00	0.00	1.47	0.00	Guangya Bank	0.00	0.00	0.00	14.70	Haima Bank	0.00	0.00	0.00	55.41
Niuchelun Reef	0.00	0.00	1.66	0.03	Wanan Bank	0.00	0.00	0.00	14.95	Chang Bank*	0.00	0.00	3.86	53.53
Nantong Reef	0.00	0.00	1.93	0.00	Gongzhen Reef*	0.00	0.00	7.27	7.74	Ao'nan Shoal*	0.00	0.00	0.00	58.76
Nanwei Island	0.23	0.00	1.33	0.42	Bayue Reef	0.00	0.00	7.08	8.12	Bai Reef	0.02	0.00	0.00	36.88
Haifan Reef	0.00	0.00	2.01	0.00	Wumie Reef	0.01	0.00	9.47	5.73	Mahu Island*	0.13	0.05	1.66	58.31
Lusha Reef	0.00	0.00	2.02	0.10	Zhubi Reef	4.43	0.00	3.89	8.06	Dayuan Bank	0.00	0.00	0.00	69.80
Zhong Reef	0.10	0.00	1.57	0.48	Haikang Shoal*	0.00	0.00	0.00	17.09	Jiuzhang Reefs**	0.46	0.05	46.27	24.34
Fulusi Reef	0.00	0.00	2.43	0.00	Renjun Bank	0.00	0.00	0.00	18.00	Daonings Reefs**	0.14	0.04	14.54	57.80
Xiyue Island	0.21	0.13	1.83	0.44	Nanhai Reef	0.05	0.00	13.39	4.87	Liumen Reef	0.04	0.00	0.00	27.97
Pengbo Shoal	0.00	0.00	1.69	1.35	Lesi Shoal	0.00	0.00	0.00	18.79	Wufang Reef	0.00	0.00	12.59	63.46
Huanglu Reef	0.00	0.00	2.36	0.68	Kangxi Shoal*	0.00	0.00	0.47	18.67	Zhongxiao Bank*	0.00	0.00	81.34	
Mengyi Shoal	0.00	0.00	3.29	0.00	Xian'e Reef	0.00	0.00	13.02	7.12	Xianbin Reef	0.00	0.00	17.43	69.45
Haikou Reef	0.00	0.00	2.12	1.39	Daxian Reef	0.09	0.00	19.49	1.83	Zhenghe Reefs**	1.00	0.36	26.14	64.34
Xiwei Bank	0.01	0.00	3.91	0.00	Shuangzi Reefs**	0.47	0.23	11.11	11.73	Yongshu Reef	2.92	0.00	23.46	81.02
Boji Reef	0.04	0.00	3.90	0.83	Lizun Bank	0.00	0.00	0.00	24.62	Southern Bank*	0.00	0.00	0.00	110.56
Yinbo Shoal*	0.01	0.00	4.23	1.59	Siling Reef	0.01	0.00	18.50	6.20	Liyue Bank	0.00	0.00	0.00	114.22
Huoai Reef	0.00	0.00	5.57	0.72	Nanhua Reef	0.03	0.00	16.22	13.56	Andu Bank*	0.03	0.00	8.60	134.08
Huayang Reef	0.26	0.00	5.50	1.65	Yongdeng Shoal	0.00	0.00	0.00	34.09	Yuya Shoal*	0.00	0.00	63.00	130.82
Xinyi Reef	0.00	0.00	5.83	2.02	Dong Reef	0.03	0.00	20.43	19.11	Total	17.93	1.13	1.13	187.25

S_i is the area of the islands/sandbanks, S_v is the area of vegetation, S_f is the area of the reef flats, and S_u is the area of the underwater part.

4.3. Geomorphic zones and areal statistics of coral reefs in the Spratly Islands

The areas of four geomorphic units are illustrated in Figs. 6–9. The areas of each class were also calculated (S_i is the area of islands/sandbanks, S_v is the area of vegetation, S_f is the area of reef flats, and S_u is the underwater area; Table 1). Note that the areas of lagoons of large atoll groups (indicated by two asterisks in Table 1) were excluded from the results because the lagoons are closely connected to the sea and cannot be accurately discriminated based on visual interpretation. In addition, it should be noted that the areas of reefs/shoals/banks that are developed on the same base (indicated by a single asterisk in Table 1) were integrated into a single entity because it is impossible to separate them underwater.

The spatial organization of the coral reefs in the Spratly Islands can be categorized into two classes: clustered and isolated. There are five atoll groups in the Spratly Islands: Shuangzi Reefs, Zhongye Reefs, Jiuzhang Reefs, Daoming Reefs and Zhenghe Reefs (in order of area, from small to large), and their total areas (i.e., the sum of islands/sandbanks, reef flats and underwater parts) are 23.31, 46.04, 71.07, 72.48, and 91.48 km², respectively. The proportion of the underwater part increases with the increasing size of the atoll group. In addition, there are 43 coral reefs with exposed areas in the Spratly Islands (23 of them are isolated), with areas ranging from 0.01 km² to 5.94 km². The areas of islands/sandbanks that are composed of atoll groups or are developed on the same base underwater are listed individually in Table S4 of the [Supplementary Material](#). The three largest artificial islands (determined by visual inspection from historical GE high resolution images) are Meiji Reef, Yongshu Reef and Zhubi Reef (from large to small) and their respective areas are 5.94, 4.43, and 2.92 km². The three largest natural islands are Taiping Island, Zhongye Island and Nanzi Island, with respective areas of 0.55, 0.47, and 0.25 km². There are a total of 47 isolated coral reefs in the Spratly Islands, with areas ranging from 0.43 km² to 107.39 km². Among them, the three with the largest reef flat areas are Bai Reef, Liumen Reef, and Xi Reef, with respective areas of 36.88, 27.97, and 25.62 km².

5. Discussion

5.1. Validation of inundation frequency with bathymetric data

In order to assess the transferability of the proposed methodology, we used it to map the inundation of coral reefs in the Great Barrier Reef (GBR)—the world's largest coral reef system. The validation was not carried out in the Spratly Islands due to the lack of field data and bathymetric data over the area. The cloud-free frequency of OLI images in the GBR is significantly higher than that in the Spratly Islands, which guarantees improved temporal coverage during the observation period. The bathymetric data provided for GBR combined the latest single-beam echo-sounder data and Lidar bathymetric survey results, and provided a spatial resolution of 100 m (Beaman, 2010). The dataset depicts the topography of GBR, including both below-surface ocean bottom (negative values) and above-surface reefs (positive values). For consistency, we used the word “bathymetry” from the original dataset to describe this data in Fig. 10. We used the dataset to determine whether the variation of inundation frequency was consistent with the water depth of the coral reefs (pixels with positive values in bathymetric data were excluded). Owing to the difference in spatial resolution between the validation data and OLI images, the bathymetric data first needed to be resampled to 30-m resolution. Correlation analysis between inundation frequency and water depth was then performed at three randomly selected test sites in the extent of the selected tile (Path/Row: 094/073). The fitting accuracy may be related to the following two factors: (i) Resampling of the validation data. The resampling technique used here was bilinear interpolation, which smoothed the data when resampling low spatial resolution image to produce a higher

spatial resolution (Parker et al., 1983). (ii) Distribution of points. The inundation frequency did not start from 0 as a result of thresholding and the relatively concentrated distribution of points probably suppressed the effect of the regression. There is a strong linear correlation between inundation frequency and water depth, with the R² values of the regression equations ranging from 0.74 to 0.78 (Fig. 10d1–3), which indicates that the inundation frequency derived from time-series OLI images reliably depicted the variation of water depth around the coral reef.

5.2. Potential limitations of the inundation mapping methodology

The method of mapping the inundation frequency of coral reefs presented herein is based on the following assumptions: (i) High-quality OLI images with adequate geometric accuracy were available so that the extraction results of inundation from different images could be accumulated directly; (ii) The extracted boundaries from each image that delineate the maximum penetration depth of optical bands exactly represent the boundaries between coral reefs and seawater; (iii) A sufficient number of satellite images taken at various water levels could be collected that enable the production of quantitative and continuous time series which can represent the geomorphology of the coral reefs; and (iv) The variation of topography (caused by the growth or degradation of coral reefs) during the observation period could be largely ignored. In a few cases, however, the geomorphology of some sandbanks exhibited high instability with unpredictable trends during the 24-year observation period (Fig. S11 of the [Supplementary Material](#)). Moreover, optically active constituents such as Colored Dissolved Organic Matter (CDOM), Total Suspended Matter (TSM), and etc. that could affect the penetration depth of visible light should be explored in future study (Cao et al., 2019). Furthermore, uncertainties in data processing and classification procedures could potentially introduce errors into the final inundation maps. These uncertainties are summarized as follows:

- (1) *Data pre-processing errors.* The effect of atmospheric and radiation attenuation in the water body could obscure the underwater signals of coral reefs. The identification of target coral reefs was based on the difference in their reflectance compared to the surrounding water, while the contrast in some images was seriously affected by noise (e.g., clouds, waves, and sun glint). Admittedly, air-water interface correction was not performed to eliminate the optical signal attenuation caused by the water column; and neither was sun glint nor waves removed, which may result in misidentification. However, the method of time-series accumulation may mitigate the interference of random noise effects. Moreover, the cloud masking method mainly depends on the reliability and stability of the OLI QA band. Nevertheless, it was found that the QA band sometimes incorrectly recognized sandbanks and other exposed objects as clouds, which would result in a lower inundation frequency in sandbank/construction areas. All of these distortions prevent the automatic calculation of coral reef inundation-frequency and require laborious visual inspection.
- (2) *Extraction errors.* The performance of the extraction algorithm to determine the boundaries of inundated areas may have some influence on the final results. As has been pointed out previously, the FCM algorithm is insensitive to spatial intensity heterogeneity (Ahmed et al., 2002). Moreover, the selection principle of initial clustering centers (which was calculated here using other clustering methods such as maximum likelihood) and the number of objective clusters (which was based on the size of the target areas in this study) would also influence the classification results. Other techniques such as mathematical morphological approaches can also be considered in order to refine the edges and shapes of the extraction results (Rishikeshan and Ramesh, 2018).
- (3) *Uneven data usability.* The inundation frequency computed here

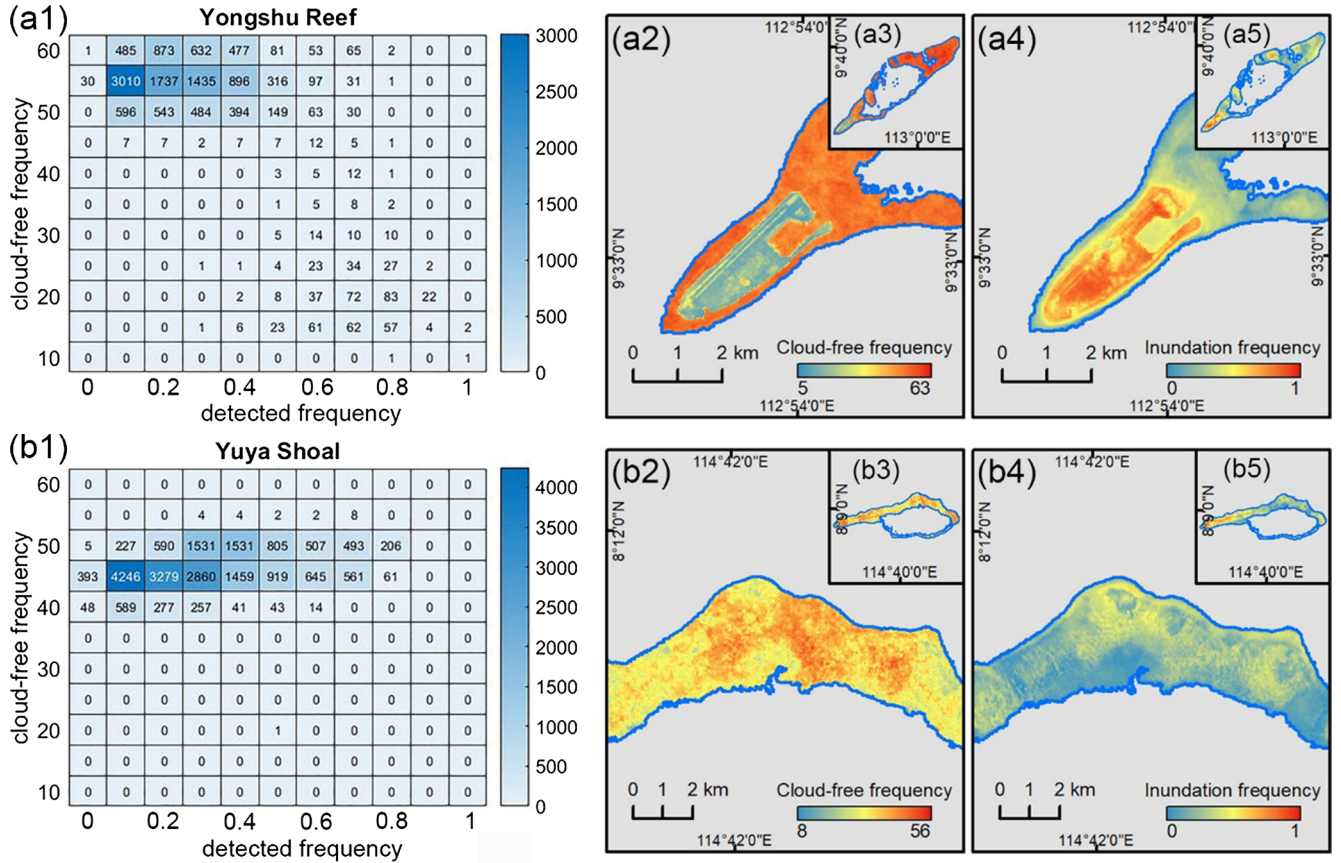


Fig. 11. (a1–b1) Heatmap chart of cloud-free frequency and detected frequency by pixels for Yongshu Reef and Yuya Shoal. The numbers in boxes are pixel counts. (a2–a5), (b2–b5) Comparison between data acquisition frequency and detected inundation frequency for Yongshu Reef and Yuya Shoal.

refers to the probability of detected inundation, which is not the actual frequency of inundation due to the limited amount of available data. In practice, the differences in data acquisition frequency between different locations may result in an uneven frequency of detected inundation. By dividing the acquisition frequency of cloud-free data for the purpose of normalization, the probability of inundation would be overestimated for relatively high topography, and underestimated for relatively low topography for areas with lower data acquisition frequency (Fig. 11). Sentinel-2 Multispectral Instrument (MSI) images with higher spatio-temporal resolution were not used in this study because of large data volume and the co-registration issue between MSI and OLI images (Storey et al., 2016). In the future, time-series MSI images involved will further improve the coral reef inundation frequency.

- (4) **Area distortion of optical RS images.** Coral reef areas were assessed based simply on the count of pixel numbers and we did not consider the area distortion caused by variation in the slope of the underwater topography. This shortcoming cannot be overcome currently owing to the restriction of optical RS.

5.3. Quantification of morphological characteristics of atolls

There are 30 isolated atolls widely distributed among the Spratly Islands. A quantitative analysis was accomplished to explore the natural process of evolution of atolls. The area (S) and perimeter (P), as well as the width of atolls (measured by the length of long axis and short axis, A_l and A_s , respectively) can be easily calculated from the time-series inundation maps (Table 2). The index of compactness (C) and extension ratio (E) can be used to characterize the morphology of atolls; they are defined as follows (Liu, 2001):

$$C = 2\sqrt{\pi S/P} \quad (5.1)$$

$$E = A_l/A_s \quad (5.2)$$

Ring-shaped reef flats are extended around the atoll lagoons. The contrast in reflectance between lagoons and the surrounding water was less apparent than for the high-reflectance reef flats and the lagoons of isolated atolls which can be extracted by visual interpretation. The ratio of lagoon area (S_l) and reef flat area (S_r) was calculated to characterize the degree of openness (O) of atolls (Table 2, ranked in ascending order). It was found that the width ratios between reef flats and lagoons decreased gradually as the value of O increased (Fig. 12), which means that atolls with a higher degree of openness are less developed (i.e., the widths of reef flats are relatively narrow). In addition, the inundation frequency of lagoons was observed to fluctuate between 0.2 and 0.4 for atolls with lower values of O (Fig. 12a–d), while the inundation frequency of lagoons did not appear to exceed 0.1 for atolls with higher values of O (Fig. 12e–h), which implies a probable correlation between openness and the water depth of lagoons.

Other morphological characteristics such as the number of entrances and the existence of patch reefs in the lagoons are listed in Table 2. The statistics indicate that the degree of openness is also related to the degree and rate of water exchange of lagoons. Relatively open atolls have one or several entrances which exchange water with the external sea and a large portion of them are frequently submerged (e.g., Yuya Shoal). By contrast, relatively closed atolls are generally unbroken or have no entrances for water exchange, and their reef flats are almost exposed at low tide (e.g., Boji Reef). Patch reefs are more likely to develop in relatively open lagoons because the secretions of corals accumulating at the bottom of lagoons can be accelerated by water fluxes. For highly developed atolls (e.g., Xianbin Reef), small and isolated patch reefs may grow into larger reefs.

Table 2

Geomorphic parameters of isolated atolls in the Spratly Islands.

Name	S_l (km ²)	S_f (km ²)	S (km ²)	P (km)	A_l (km)	A_s (km)	O	C	E	Entrance number	Patch Reefs (Y/N)
Huo'ai Reef	0.26	5.57	6.28	29.33	5.39	1.76	0.05	1.64	3.06	0	N
Daxian Reef	1.83	19.49	21.40	40.56	14.68	1.78	0.09	2.58	8.25	1*	N
Boji Reef	0.83	3.90	4.77	10.86	3.18	1.95	0.21	2.35	1.63	0	N
Riji Reef	1.61	7.43	9.99	19.98	6.15	1.86	0.22	2.51	3.31	0	N
Bisheng Reef	2.57	10.46	13.93	27.76	9.17	2.21	0.25	2.51	4.15	1*	N
Huanglu Reef	0.68	2.36	3.04	8.73	2.19	1.61	0.29	2.09	1.35	0	N
Siling Reef	6.20	18.50	24.71	36.56	10.67	2.91	0.34	2.91	3.67	0	N
Xinyi Reef	2.02	5.83	7.85	18.91	6.74	1.29	0.35	2.28	5.21	0	N
Nanhai Reef	4.87	13.39	18.30	33.04	9.95	2.67	0.36	2.64	3.72	1*	N
Sanjiao Reef	3.55	8.17	12.02	22.37	4.77	3.39	0.43	2.60	1.41	0	N
Xi Reef	12.94	25.62	42.08	41.64	10.34	5.66	0.50	3.56	1.83	9	Y
Bai Reef	18.75	36.88	59.01	82.72	28.46	3.81	0.51	2.99	7.47	0	Y
Xian'e Reef	7.12	13.02	20.14	24.84	7.85	3.58	0.55	3.19	2.19	0	N
Wumie Reef	5.73	9.47	15.22	21.57	6.94	3.14	0.61	2.98	2.21	0	N
Haikou Reef	1.32	2.12	3.51	9.04	2.62	1.72	0.62	2.21	1.53	0	Y
Guangxing Reef	5.37	8.51	13.88	25.26	9.23	1.76	0.63	2.63	5.24	0	N
Pengbo Shoal	1.29	1.69	3.04	8.81	2.30	1.49	0.76	2.08	1.54	0	N
Danwan Reef	4.68	5.93	11.06	20.64	7.41	2.22	0.79	2.59	3.34	2*	Y
Nanhua Reef	13.56	16.22	29.81	33.31	8.73	3.83	0.84	3.35	2.28	2*	Y
Dong Reef	19.11	20.43	39.56	39.54	12.51	3.48	0.94	3.55	3.59	1	Y
Jianzhang Reef	4.56	4.52	9.14	15.01	4.39	2.60	1.01	2.77	1.69	0	Y
Banyue Reef	7.82	7.08	15.20	23.86	4.94	3.13	1.10	2.83	1.58	1	Y
Renai Reef	26.61	18.35	50.81	50.93	16.76	4.69	1.45	3.54	3.57	8	Y
Liumen Reef	41.54	27.97	74.00	66.72	18.81	5.37	1.48	3.73	3.50	9	Y
Yuya Shoal	96.67	63.00	193.82	120.42	31.84	11.05	1.53	4.50	2.88	4	Y
Zhubi Reef	7.01	3.89	16.38	22.74	5.31	3.84	1.80	3.01	1.38	1*	N
Yongshu Reef	47.07	23.46	107.39	130.92	26.16	7.24	2.01	3.21	3.61	5	Y
Xianbin Reef	51.32	17.43	86.88	148.54	18.13	7.00	2.94	2.71	2.59	19	Y
Wufang Reef	44.03	12.59	76.05	93.93	9.96	8.61	3.50	3.19	1.16	5	N
Meiji Reef	31.50	7.78	47.39	34.29	9.30	6.14	4.05	4.17	1.51	2*	N

Numbers marked with an asterisk indicate artificially-constructed entrances. S_l is the area of lagoon; S_f is the area of reef flats; S is the total area; P is the perimeter; A_l and A_s are the long and short axes, O is the openness, C is the compactness, and E is the extensive ratio.

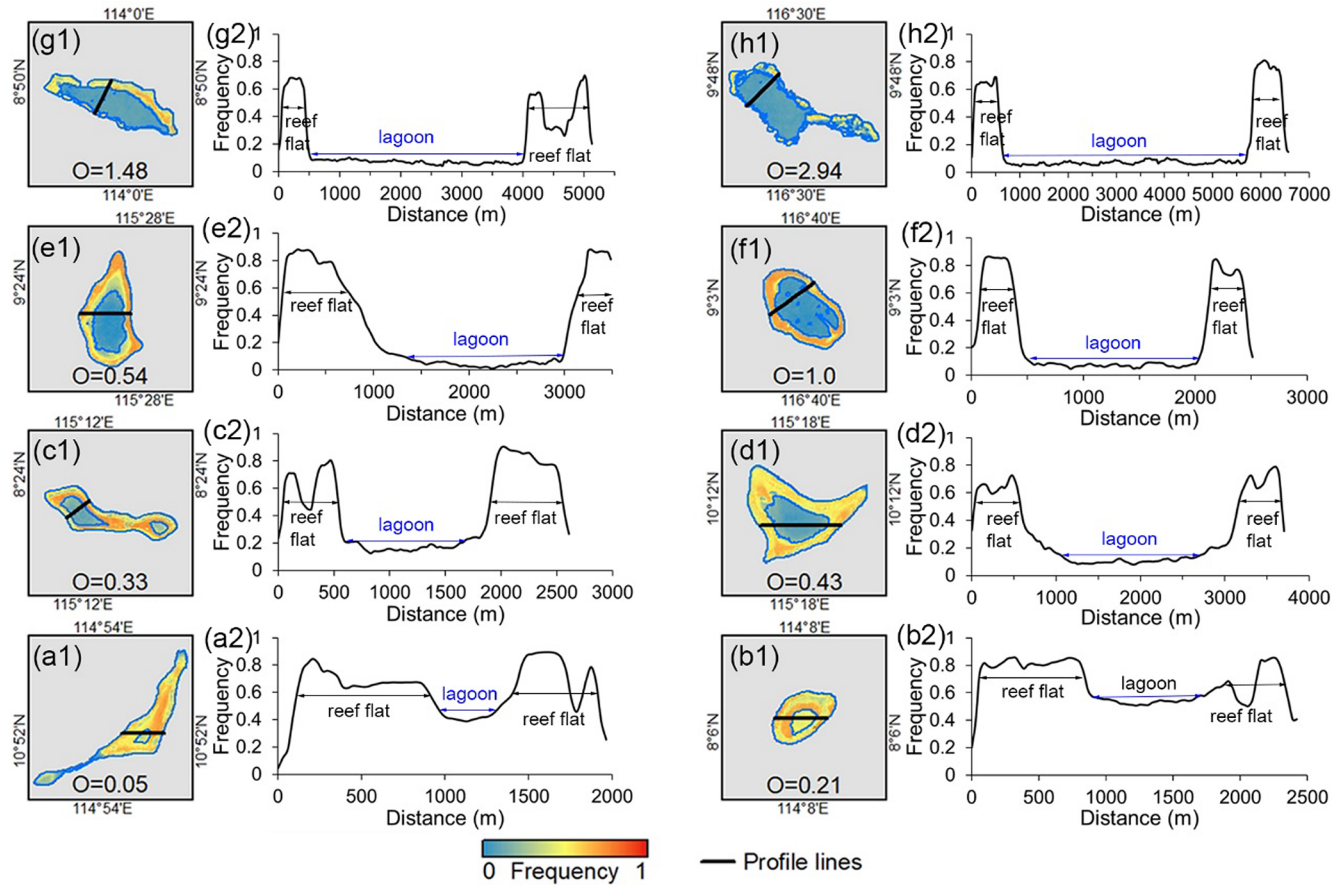


Fig. 12. (a1–h1) Inundation frequency of isolated atolls (ranked by degree of openness) in the Spratly Islands. (a2–h2) Selected inundation profiles across the reefs.

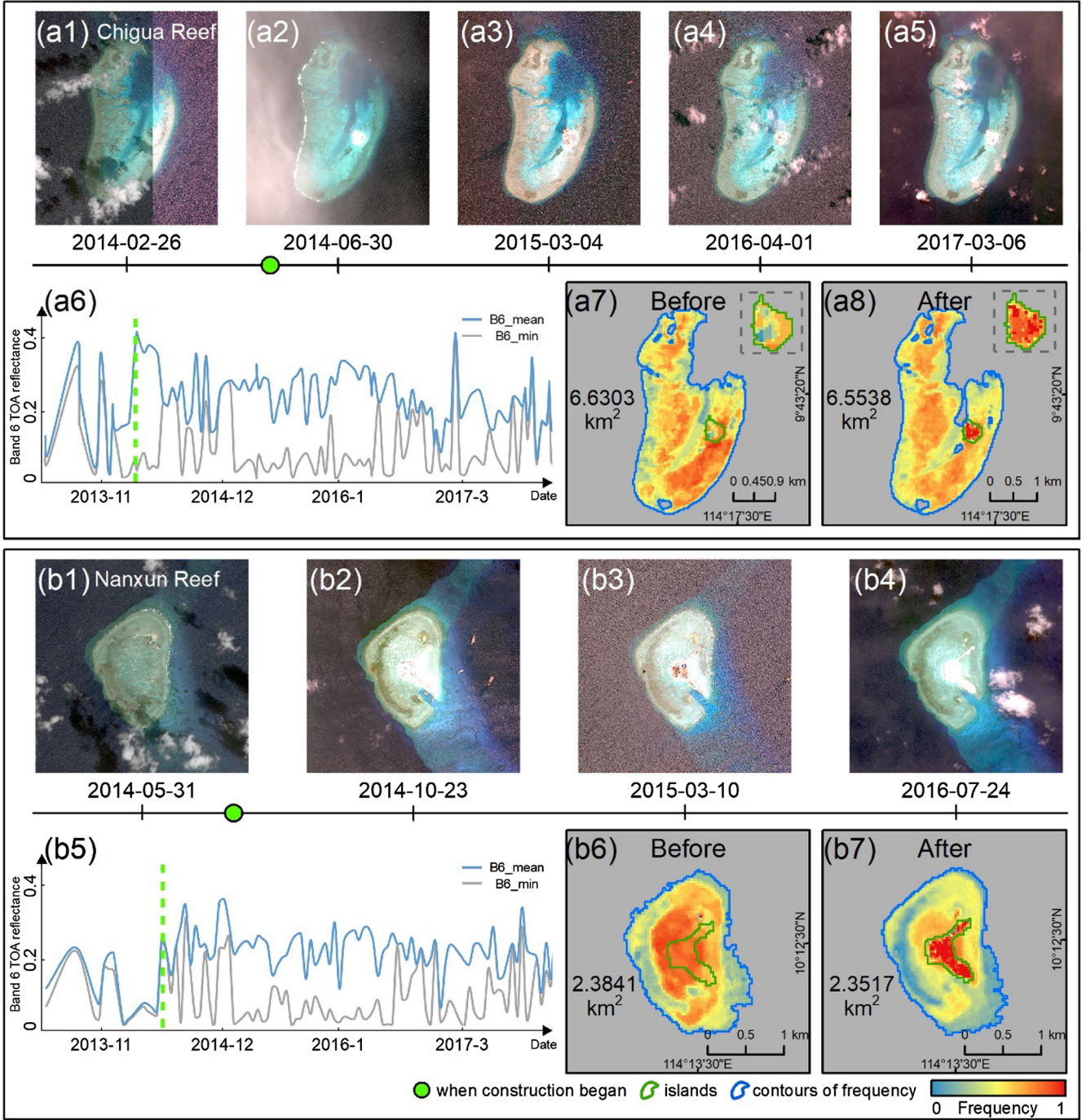


Fig. 13. (a1–a5, b1–b4) Time-series of HR images of Chigua Reef and Nanxun Reef. (a6, b5) Time-series chart of mean and minimum values of OLI band 6 TOA reflectance of exposed areas in Chigua Reef and Nanxun Reef. (a7–a8, b6–b7) Inundation frequency of Chigua Reef and Nanxun Reef before and after construction (the start dates of construction are 26 May 2014 and 30 August 2014 for Chigua Reef and Nanxun Reef, respectively). Boundaries of areas within the same frequency range are shown in blue. The areas of coral reefs within the same frequency range decreased slightly after construction. (For interpretation of the references to color in this figure legend, the reader is referred to the web version of this article.)

5.4. Effects of reclamation on coral reefs

Small sandbanks and islands piling up on the surface of reef flats are exposed to the air in most cases and therefore they should exhibit the highest frequency in the inundation maps. The vegetation developed on them is regarded as a scarce and valuable resource. In visible light bands, however, vegetated areas usually exhibit lower reflectance than the surrounding submerged coral reefs and they generate ‘holes’ (i.e., abnormal low inundation frequency) on the islands in the inundation maps. In order to rectify this problem, the occurrence of exposed areas

(e.g., rocks, natural sandy islands, artificial islands, sandbanks and even anchored ships) in OLI Bands 2–4 were acknowledged as long as they were extracted from OLI Band 6 (Fig. S3c of the Supplementary Material).

Notably, a careful inspection of exposed areas in the final inundation maps revealed that the inundation frequency of artificial islands (inspected from historical GE high resolution images) is lower than that of natural islands. Since most artificial islands were constructed halfway through the time period from 2013 to 2015 (Barnes and Hu, 2016), it was impossible for them to appear at the beginning of the time

series. To illustrate this point, a visual examination was conducted of several artificial islands in historical GE HR images in order to monitor their process of construction (Fig. 13a1–5, b1–4). Also, time-series charts of average Band 6 TOA reflectance within the exposed areas were generated using Google Earth Engine (GEE) API in order to determine the exact starting date of reclamation (GEE is not used for computing in the present study, mainly because the fuzzy classification adopted herein cannot be conducted in parallel in GEE) (Fig. 13a6, b5). Two phases of inundation maps—before and after reclamation—could be separated according to the start date. The inundation frequency of artificial islands, by comparison, has substantially increased after reclamation (Fig. 13a7–8, b6–7). Interestingly, we also found that the inundation frequency of the corresponding coral reef areas near the reclamation areas after reclamation was significantly lower than before (Fig. 13a7–8, b6–7). Considering the fact that the construction of artificial islands in some coral reef areas was accomplished by the method of transferring coral sand from neighboring coral reef flat/bodies to the artificial island area by pumping, we infer that those areas exhibiting a decrease of inundation frequency around reclamation areas may indicate the spatial extent of coral reefs damaged by human activities. This may be another form of indirect evidence that demonstrates the robustness of the proposed method for mapping coral reef inundation frequency.

6. Conclusion

Coral reef habitat maps and bathymetry data for disputed areas are usually poorly available. Here, a simple method is proposed for mapping the geomorphological characteristics of coral reefs by using time-series Landsat-8 OLI images without *in situ* measurements. The method employs the reef-water reflectance contrast characteristic—varying with bathymetry, bands, and water level—documented in time-series of optical multi-band images. This enabled the inundation frequency and geomorphic zonation of coral reefs in the Spratly Islands to be determined. A detailed and novel inventory that includes the spatial extent, inundation frequency, and geomorphic zones of coral reefs of this disputed marine area has been established. The inundation frequency of reef flats around reclaimed areas before and after island construction is different, which may reflect anthropogenic influences on the coral reef systems. Validation in the Great Barrier Reef (Australia) suggested that the inundation frequency of coral reefs derived by the proposed method may serve as an indirect representation of bathymetry in coral reef areas. In the future, the combination of field data, Landsat-8 OLI and optical images acquired by other sensors (e.g., Sentinel-2 A/B multispectral instrument) hopefully can provide enhanced temporal resolution multi-spectral images for the global mapping and monitoring of coral reef ecosystem at finer scale, with the consideration of registration of images from multiple sources.

Acknowledgments

This research is supported by National Natural Science Foundation of China (Grant no. 41971378) and the Jiangsu Provincial Natural Science Foundation (Grant no. BK20160023). The authors are grateful to the United States Geological Survey (USGS) for providing all Landsat-8 OLI images used. Note that any errors or shortcomings in the paper are the responsibility of the authors.

Appendix A. Supplementary material

Supplementary data to this article can be found online at <https://doi.org/10.1016/j.isprsjprs.2019.09.011>.

References

- Ahmad, W., Neil, D.T., 1994. An evaluation of Landsat Thematic Mapper (TM) digital data for discriminating coral reef zonation: Heron Reef (GBR). *Int. J. Remote Sens.* 15, 2583–2597.
- Ahmed, M.N., Yamany, S.M., Mohamed, N., Farag, A.A., Moriarty, T., 2002. A modified fuzzy c-means algorithm for bias field estimation and segmentation of MRI data. *IEEE Trans. Med. Imaging* 21, 193–199.
- Andréfouët, S., Muller-Karger, F.E., Robinson, J.A., Kranenburg, C.J., Torres-Pulliza, D., Spraggins, S.A., Murch, B., 2006. Global assessment of modern coral reef extent and diversity for regional science and management applications: a view from space. In: Proceedings of the 10th International Coral Reef Symposium, Okinawa, Japan, pp. 1732–1745.
- Barkley, H.C., Cohen, A.L., Golbuu, Y., Starczak, V.R., DeCarlo, T.M., Shamberger, K.E.F., 2015. Changes in coral reef communities across a natural gradient in seawater pH. *Sci. Adv.* 1, e1500328.
- Barnes, B.B., Hu, C., 2016. Island building in the South China Sea: detection of turbidity plumes and artificial islands using Landsat and MODIS data. *Sci. Rep.* 6, 33194.
- Beaman, R.J., 2010. Project 3D-GBR: A high-resolution depth model for the Great Barrier Reef and Coral Sea. Marine and Tropical Sciences Research Facility (MTSRF) Project 2.5i.1a Final Report, MTSRF, Cairns, Australia, pp. 13 plus Appendix 1. <https://www.deepreef.org/bathymetry/65-3dgb-bathy.html>.
- Bellwood, D.R., Hughes, T.P., Folke, C., Nyström, M., 2004. Confronting the coral reef crisis. *Nature* 429, 827–833.
- Brock, J.C., Wright, C.W., Kuffner, I.B., Hernandez, R., Thompson, P., 2006. Airborne lidar sensing of massive stony coral colonies on patch reefs in the northern Florida reef tract. *Remote Sens. Environ.* 104, 31–42.
- Butchart, S.H.M., Walpole, M., Collen, B., van Strien, A., Scharlemann, J.P.W., Almond, R.E.A., Baillie, J.E.M., Bomhard, B., Brown, C., Bruno, J., Carpenter, K.E., Carr, G.M., Chanson, J., Chinery, A.M., Csirke, J., Davidson, N.C., Dentener, F., Foster, M., Galli, A., Galloway, J.N., Genovesi, P., Gregory, R.D., Hockings, M., Kapos, V., Lamarque, J., Leverington, F., Loh, J., McGeoch, M.A., McRae, L., Minasyan, A., Morcillo, M.H., Oldfield, T.E.E., Pauly, D., Quader, S., Revenga, C., Sauer, J.R., Skolnik, B., Spear, D., Stanwell-Smith, D., Stuart, S.N., Symes, A., Tierney, M., Tyrrell, T.D., Vié, J., Watson, R., 2010. Global biodiversity: indicators of recent declines. *Science* 328, 1164–1168.
- Cao, Z., Ma, R., Duan, H., Xue, K., 2019. Effects of broad bandwidth on the remote sensing of inland waters: Implications for high spatial resolution satellite data applications. *ISPRS J. Photogramm. Remote Sens.* 153, 110–122.
- Chen, B., Yang, Y., Xu, D., Huang, E., 2019. A dual band algorithm for shallow water depth retrieval from high spatial resolution imagery with no ground truth. *ISPRS J. Photogramm. Remote Sens.* 151, 1–13.
- Cinner, J.E., McClanahan, T.R., MacNeil, M.A., Graham, N.A.J., Daw, T.M., Mukminin, A., Feary, D.A., Rabearisoa, A.L., Wamukota, A., Jiddawi, N., Campbell, S.J., Baird, A.H., Januchowski-Hartley, F.A., Hamed, S., Lahari, R., Morove, T., Kuange, J., 2012. Comanagement of coral reef social-ecological systems. *Proc. Natl. Acad. Sci.* 109, 5219–5222.
- De'ath, G., Fabricius, K.E., Sweatman, H., Puotinen, M., 2012. The 27-year decline of coral cover on the Great Barrier Reef and its causes. *Proc. Natl. Acad. Sci.* 201208909.
- Dodge, R.E., Vaišnys, J.R., 1975. Hermatypic coral growth banding as environmental recorder. *Nature* 258, 706–708.
- Gardner, T.A., Côté, I.M., Gill, J.A., Grant, A., Watkinson, A.R., 2003. Long-term region-wide declines in Caribbean corals. *Science* 301, 958–960.
- Geographical Names Committee of Guangdong Province, 1987. Compilation of geographical names of the South China Sea Islands. Cartographic Publishing House, Guangdong province (In Chinese).
- Ghosh, A., Mishra, N.S., Ghosh, S., 2011. Fuzzy clustering algorithms for unsupervised change detection in remote sensing images. *Inf. Sci.* 181, 699–715.
- Hoegh-Guldberg, O., Mumby, P.J., Hooten, A.J., Steneck, R.S., Greenfield, P., Gomez, E., Harvell, C.D., Sale, P.F., Edwards, A.J., Caldeira, K., Knowlton, N., Eakin, C.M., Iglesias-Prieto, R., Muthiga, N., Bradbury, R.H., Dubi, A., Hatzinikolas, M.E., 2007. Coral reefs under rapid climate change and ocean acidification. *Science* 318, 1737–1742.
- Jaap, W.C., 2000. Coral reef restoration. *Ecol. Eng.* 15, 345–364.
- Jung, W., Vogt, P.R., 1992. Predicting bathymetry from Geosat-ERM and shipborne profiles in the South Atlantic Ocean. *Tectonophysics* 210, 235–253.
- Jupp, D.L.B., 1988. Background and extensions to depth of penetration (DOP) mapping in shallow coastal waters. In: Proceedings of the Symposium on Remote Sensing of the Coastal Zone, Gold Coast, Queensland, pp. IV 2.1–19.
- Leon, J., Woodroffe, C.D., 2011. Improving the synoptic mapping of coral reef geomorphology using object-based image analysis. *Int. J. Geogr. Inf. Sci.* 25, 949–969.
- Liu, B., 2001. Analysis and Measurement of Remote Sensing Fusion Information Characteristics in the Spratly Islands. China Ocean Press.
- Liu, Y., Hu, C., Dong, Y., Xu, B., Zhan, W., Sun, C., 2019. Geometric accuracy of remote sensing images over oceans: The use of global offshore platforms. *Remote Sens. Environ.* 222, 244–266.
- Liu, Y., Li, M., Zhou, M., Yang, K., Mao, L., 2013. Quantitative analysis of the waterline method for topographical mapping of tidal flats: A case study in the Dongsha Sandbank China. *Remote Sens.* 5, 6138–6158.
- Mulhall, M., 2009. Saving the rainforests of the sea: an analysis of international efforts to conserve coral reefs. *Duke Environ. Law Policy Forum* 19, 321–351.
- Ortiz, J., Wolff, N.H., Anthony, K.R.N., Devlin, M., Lewis, S., Mumby, P.J., 2018. Impaired recovery of the Great Barrier Reef under cumulative stress. *Sci. Adv.* 4, eaar6127.
- Parker, J.A., Kenyon, R.V., Troxel, D.E., 1983. Comparison of interpolating methods for image resampling. *IEEE Trans. Med. Imaging* 2, 31–39.
- Pauly, D., Christensen, V., Guénette, S., Pitcher, T.J., Sumaila, U.R., Walters, C.J., Watson, R., Zeller, D., 2002. Towards sustainability in world fisheries. *Nature* 418, 689–695.
- Phinn, S.R., Roelfsema, C.M., Mumby, P.J., 2012. Multi-scale, object-based image analysis for mapping geomorphic and ecological zones on coral reefs. *Int. J. Remote Sens.* 33, 3768–3797.
- Rishikeshan, C.A., Ramesh, H., 2018. An automated mathematical morphology driven

- algorithm for water body extraction from remotely sensed images. *ISPRS J. Photogramm. Remote Sens.* 146, 11–21.
- Roelfsema, C., Kovacs, E., Ortiz, J.C., Wolff, N.H., Callaghan, D., Wettle, M., Ronan, M., Hamylton, S.M., Mumby, P.J., Phinn, S., 2018. Coral reef habitat mapping: A combination of object-based image analysis and ecological modelling. *Remote Sens. Environ.* 208, 27–41.
- Shinn, E.A., 1966. Coral growth-rate, an environmental indicator. *J. Paleontol.* 40, 233–240.
- Smith, S.V., 1978. Coral-reef area and the contributions of reefs to processes and resources of the world's oceans. *Nature* 273, 225–226.
- Stone, R., 2010. Earth-observation summit endorses global data sharing. *Science* 330, 902.
- Storey, J., Roy, D.P., Masek, J., Gascon, F., Dwyer, J., Choate, M., 2016. A note on the temporary misregistration of Landsat-8 Operational Land Imager (OLI) and Sentinel-2 Multi Spectral Instrument (MSI) imagery. *Remote Sens. Environ.* 186, 121–122.
- Su, J., 2004. Overview of the South China Sea circulation and its influence on the coastal physical oceanography outside the Pearl River Estuary. *Cont. Shelf Res.* 24, 1745–1760.
- Townshend, J.R.G., Justice, C.O., 1986. Analysis of the dynamics of African vegetation using the normalized difference vegetation index. *Int. J. Remote Sens.* 7, 1435–1445.
- UNEP-WCMC, WorldFish Centre, WRI, TNC, 2018. Global distribution of warm-water coral reefs, compiled from multiple sources including the Millennium Coral Reef Mapping Project. Version 4.0. <http://data.unep-wcmc.org/datasets/1>.
- USGS, 2018. Landsat 8 Data Users Handbook. https://landsat.usgs.gov/sites/default/files/documents/LSDS-1574_L8_Data_Users_Handbook.pdf, Accessed date: 1 February 2019.
- Wang, L., Yu, K., Zhao, H., Zhang, Q., 2014. Economic valuation of the coral reefs in South China Sea. *Tropical Geography* 34, 44–49.
- Wang, Y., Liu, Y., Jin, S., Sun, C., Wei, X., 2019. Evolution of the topography of tidal flats and sandbanks along the Jiangsu coast from 1973 to 2016 observed from satellites. *ISPRS J. Photogramm. Remote Sens.* 150, 27–43.
- Wulder, M.A., Masek, J.G., Cohen, W.B., Loveland, T.R., Woodcock, C.E., 2012. Opening the archive: How free data has enabled the science and monitoring promise of Landsat. *Remote Sens. Environ.* 122, 2–10.
- Yang, Y., Liu, Y., Zhou, M., Zhang, S., Zhan, W., Sun, C., Duan, Y., 2015. Landsat 8 OLI image based terrestrial water extraction from heterogeneous backgrounds using a reflectance homogenization approach. *Remote Sens. Environ.* 171, 14–32.
- Zhao, J., Barnes, B., Melo, N., English, D., Lapointe, B., Muller-Karger, F.E., Schaeffer, B., Hu, C., 2013. Assessment of satellite-derived diffuse attenuation coefficients and euphotic depths in south Florida coastal waters. *Remote Sens. Environ.* 131, 38–50.
- Zhang, C., 2015. Applying data fusion techniques for benthic habitat mapping and monitoring in a coral reef ecosystem. *ISPRS J. Photogramm. Remote Sens.* 104, 213–223.
- Zhong, J., 1996. Study of Coral Reef Geomorphology in the Spratly Islands. Science Press.